Harmonic resonant excitation of flow-distributed oscillation waves and Turing patterns driven at a growing boundary

Patrick N. McGraw,[1] Michael Menzinger,[1] and Alberto P. Muñuzuri[2]
[1]*Department of Chemistry, University of Toronto, Toronto, Ontario, Canada M5S 3H6*
[2]*Grupo de Física Non Lineal, Universidade de Santiago de Compostela, A Coruña, 15782 Santiago de Compostela, Spain*
(Received 12 November 2008; published 20 August 2009)

We perform numerical studies of a reaction-diffusion system that is both Turing and Hopf unstable, and that grows by addition at a moving boundary (which is equivalent by a Galilean transformation to a reaction-diffusion-advection system with a fixed boundary and a uniform flow). We model the conditions of a recent set of experiments which used a temporally varying illumination in the boundary region to control the formation of patterns in the bulk of the photosensitive medium. The frequency of the illumination variations can select patterns from among the competing instabilities of the medium. In the usual case, the waves that are excited have frequencies (as measured at a constant distance from the upstream boundary) matching the driving frequency. In contrast to the usual case, we find that both Turing patterns and flow-distributed oscillation waves can be excited by forcing at subharmonic multiples of the wave frequencies. The final waves (with frequencies at integer multiples of the driving frequency) are formed by a process in which transient wave fronts break up and reconnect. We find ratios of response to driving frequency as high as 10.

DOI: 10.1103/PhysRevE.80.026209 PACS number(s): 05.45.−a, 82.40.Ck, 47.54.−r

I. INTRODUCTION

A system with a convective instability [1,2] allows the possibility of pattern formation controlled by the upstream boundary condition, since effects of the boundary grow with downstream distance, whereas the results of initial conditions are eventually swept downstream and out of the reactor. A particularly interesting example of pattern formation controlled by an upstream boundary is the so-called flow-distributed oscillation (FDO) mechanism, which occurs when the chemical medium undergoes a self-sustained oscillation as it flows [3–6]. The essential mechanism of FDO is that the phase of the chemical oscillator is set at the upstream boundary, and the oscillations of each fluid element as it is advected downstream result in recurring phase fronts at periodic downstream positions. If the boundary condition is stationary, then the waves are stationary [3,7,8], whereas steadily oscillating boundary conditions can result in either upstream or downstream traveling waves [4,6,9].

A flow system with a fixed boundary is equivalent via a Galilean transformation to a stationary medium with a moving (growing) boundary [4,9] and FDO has been demonstrated experimentally in both situations. One of the more exciting applications of the FDO mechanism is in biological morphogenesis, where an oscillating pacemaker at the growing tip of an embryo or plant stem can imprint a periodic pattern on the growing medium behind it [4,6,9,10]. Such a mechanism has been observed in the somitogenesis process in the chick embryo [4,9]. Laboratory experiments in chemical media have demonstrated FDO in a packed-bed reactor with a flowing medium as well as in a stationary medium with a moving boundary.

The theory was extended to include the possibility of differential flow and diffusion. Stationary structures in a general flow system with differential transport are referred to as "flow- and diffusion-distributed structures" (FDS) [11–13]. It was shown by means of linear analysis that in general two sets of modes can be excited by an appropriate oscillatory boundary condition [14]. One of these, associated with the underlying Hopf instability, comprises the FDO waves (or, if differential flow is important, there may instead be the so-called differential flow instability or DIFI) and the other set comprises Turing patterns, which are stationary with respect to the medium.[1] The essentials of this picture were confirmed in recent experiments in a stationary medium with a moving boundary, subject to strong differential diffusion [15]. FDO waves were found to be controlled by the driving frequency at the boundary, for appropriately chosen frequencies comparable to the medium's natural oscillation frequency, while at higher driving frequencies Turing patterns were excited.

Numerical simulations done in connection with the recent experiments also showed results suggesting harmonic resonances of both FDO and Turing modes, in addition to the simple FDO and Turing modes that were expected, and those resonances are the subject of this paper. What we mean here by resonance is most easily appreciated in the context of a flow system with fixed upstream boundary or, in the case of the equivalent growing system, by considering a point that remains at a constant distance from the moving boundary. This may be illustrated by examining the space-time plots of Figs. 3 and 4. (These figures will be discussed in more detail later.) In both figures, the grayscale represents a chemical concentration, and the rightward moving boundary is apparent as a diagonal across the plot. The vertical spacing of the stripes to the lower right of this diagonal represents the frequency of a driving signal applied to the right of the boundary, and wave patterns are excited in the medium to the left. In each case, the dotted white line shows the trajectory of a point moving at a constant distance behind the boundary. In Fig. 3, the frequency of the waves as measured along this

[1]In view of the strong analogy with FDO waves, we refer to Turing structures excited in this manner by the boundary as "Turing waves."

line is identical to the driving frequency, whereas in the second case (Fig. 4) it is twice the driving frequency. These two plots then show examples of two different resonances, with the frequencies of the driving signal and the resulting waves related by different integer ratios. The frequencies for which these integer ratios hold are specifically the frequencies *as measured at a constant distance behind the boundary* or at a point that is stationary *in a frame of reference where the boundary is stationary*. As explained further in the next section, this must be distinguished from the frequency as measured at a point that is stationary with respect to the medium.

Multiple integer resonances have also been seen in simulations of flow systems without differential transport, but with a sinusoidal modulation of the flow velocity [16]. As we will argue below, the essential ingredients are the same in the flow system with modulated velocity and in the system currently considered. In both cases, both boundary, with an associated steady signal, and superimposed oscillating signal are present. A different but possibly related effect was observed in simulations of the Oregonator model, where stationary waves break up into traveling waves with an integer "firing number" when the flow velocity approaches a critical value [17].

The remainder of the paper is organized as follows. In the Sec. II we briefly describe the generic FDO mechanism and introduce our notation and conventions. We find it useful to consider the system in two different frames of reference and define variables associated with both frames. In Sec. III we apply this discussion to the Lengyel-Epstein model of the photosensitive chlorine dioxide-iodide-malonic (CDIMA) reaction [18] (with parameters chosen in the range of both Hopf and Turing instabilities, in agreement with experiments) and describe our numerical simulations and the experiments on which they are based. Simulation results showing resonances are given in Sec. IV. Subsequently, in Sec. V we discuss the essential ingredients of the mechanism of resonance and argue that it is determined by topology and geometry. We interpret the breakup and the reformation of FDO waves as a type of constrained synchronization mechanism in the spatially extended reaction-diffusion system, where the tendency of diffusion to synchronize the chemical oscillation operates under constraints imposed by the periodically driven boundary conditions. Because the dynamics is attracted to the limit cycle, which is a nonsimply connected set in phase space, one can in fact apply some of the same reasoning as in the theory of topological defects familiar to field theorists and condensed-matter physicists [19].

II. FDO MECHANISM: DEFINITIONS AND NOTATION

As mentioned above, a flow system with a fixed inlet is equivalent by way of a Galilean transformation to a stationary medium with a moving boundary. The resonances we are interested in are most readily perceived in the flow system (fixed-boundary) frame of reference, as they are marked by integer ratios of frequencies as measured in this frame. Other aspects of the FDO mechanism, on the other hand, are most easily understood in terms of the moving-boundary or "growing" frame of reference. In particular, the relationships between various wave modes and underlying instabilities of the medium are best understood when the medium is stationary. Likewise, an understanding of the essential kinematics of FDO waves requires us to consider the behavior of a point that is stationary with respect to the medium rather than the boundary. The experiments that inspired the current work were performed in a stationary medium with a moving boundary. For these reasons, it is useful and sometimes necessary to switch back and forth between the two reference frames at will or to consider both simultaneously.

Therefore, we define two coordinate systems: the flow system (fixed boundary or F) position and time coordinates ξ and τ and the growth (moving boundary or M) coordinates x and t, related by the Galilean transformation

$$\xi = Vt - x,$$

$$\tau = t, \tag{1}$$

where V is the flow (or moving-boundary) velocity. Note the sign reversal between the two position coordinates, which is necessary if both the boundary velocity and the flow velocity are taken to be positive. ξ can be interpreted as a point's distance behind the advancing boundary. It is proportional to the time elapsed *since* a fluid element of the medium left the boundary, while x is proportional to the time *at which* that element left the boundary. Lines of constant x represent the trajectories of points advected along with the fluid.

Dynamical equations can be transformed from one frame to the other via the substitutions[2]

$$\frac{\partial}{\partial x} = -\frac{\partial}{\partial \xi}, \quad \frac{\partial}{\partial t} = \frac{\partial}{\partial \tau} + V\frac{\partial}{\partial \xi} \tag{2}$$

or

$$\frac{\partial}{\partial \xi} = -\frac{\partial}{\partial x}, \quad \frac{\partial}{\partial \tau} = \frac{\partial}{\partial t} - V\frac{\partial}{\partial x}.$$

A generic periodic traveling wave is described in F coordinates by a function

$$\psi(\omega_F \tau - k_F \xi), \quad \psi(\theta + 2\pi) = \psi(\theta), \tag{3}$$

where ω and k are the frequency and the wave number. ψ stands for a generic dynamical variable or vector of dynamical variables. Using Eq. (1), this wave form can be re-expressed in M coordinates as follows:

$$\psi(\omega_F \tau - k_F \xi) = \psi[\omega_F t - k_F(Vt - x)] = \psi(\omega_M t - k_M x), \tag{4}$$

where

$$\omega_M = \omega_F - k_F V \tag{5}$$

and

[2]Partial derivatives $\partial/\partial t$ and $\partial/\partial \tau$ are implicitly assumed to be taken with, respectively, x and ξ held constant. This is the main reason to distinguish the notation of the time coordinates.

$$k_M = -k_F \tag{6}$$

describe the temporal and the spatial periodicities as reckoned in the moving-boundary or the growth frame of reference. For the phase velocities $c=\omega/k$, we easily get the expected result that

$$c_M = V - c_F, \tag{7}$$

i.e., the phase velocities undergo the Galilean transformation. In the standard FDO mechanism, the waves are excited by a periodic driving at the upstream ($\xi=0$) boundary. Matching the periodicities at $\xi=0$ requires that ω_F, the frequency of the waves in the fixed-boundary frame, is equal to the driving frequency ω_D. Furthermore, if any given fluid element oscillates as it is advected (or as it stays stationary in the moving-boundary frame) with a natural frequency ω_0 determined by the chemical oscillation mechanism, then we must have $\omega_M = \omega_0$, and the periodic wave function ψ itself is determined by the chemical oscillator's limit cycle. The two conditions

$$\omega_F = \omega_D,$$

$$\omega_M = \omega_0 \tag{8}$$

along with relations (5) and (6) suffice to derive the so-called "kinematic" relations [4,6,9] for the wavelength and the phase velocity of the resulting waves. These relations may also be interpreted as expressing geometrical relationships among the spatial and the temporal periodicities of the waves and the oscillations [15]. In reality, each fluid element does not oscillate independently, but it is coupled to nearby fluid elements by diffusion, which can modify both the oscillation frequency and the shape of the limit cycle [the functional form $\psi(\theta)$] [20–22]. The kinematic relations remain valid only if ω_0 is replaced with ω_M. The latter can be interpreted as a kind of "effective natural frequency" that varies with the wavelength. In the system we study in the current work, variations in ω_M are small, so for most purposes $\omega_M=\omega_0$ =const is a good approximation.

In a medium with differential diffusion admitting Turing structures, the latter may also be selected by means of an oscillatory driving at the boundary. Turing structures by their nature are stationary with respect to the medium, so in this case $\omega_M=0$, $c_M=0$ and therefore, using Eqs. (5) and (6),

$$|k_M| = \frac{|\omega_D|}{V} \tag{9}$$

or

$$\lambda = VT_D,$$

where T_D is the driving period and λ is the pattern wavelength. The above equation means that as the boundary advances with speed V, it deposits behind itself one wavelength of the Turing pattern for each cycle of the driving oscillation, as shown in the schematic space-time diagram in Fig. 1.

In general, an oscillating dynamical system has an unstable equilibrium inside the limit cycle. An approximate description of the FDO waves that propagate into the medium from the boundary can be found by considering boundary conditions that are a small perturbation of the equilibrium

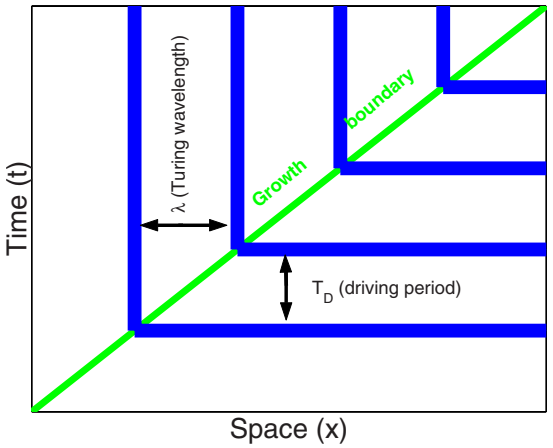

FIG. 1. (Color online) Each oscillation of the driving signal deposits one Turing wave as the boundary advances.

and deriving a dispersion relation for small-amplitude waves of the form [14,22]

$$\psi(\xi,\tau) = A \exp i(\omega_F\tau - k_F\xi), \tag{10}$$

which should match the upstream boundary condition at $\xi=0$. Since we are interested in perturbations with steady amplitude at the boundary, we therefore consider only purely real values of ω_F while k_F may be complex. A positive (negative) imaginary component of k_F means that the wave grows (damps) with increasing downstream distance. Growing waves can be expected to saturate at some finite amplitude, asymptotically approaching form (3) for large ξ. Therefore nonlinear wave solutions can be predicted (to a first approximation) on the basis of the growing modes that are found from the dispersion relation.

III. CDIMA REACTION IN A GROWING MEDIUM

We are interested in the photosensitive chlorine dioxide-iodide-malonic acid (CDIMA) reaction, which was studied in recent experiments [15]. We model the reaction mathematically by the Lengyel-Epstein [18] kinetic model, which for an effectively one-dimensional medium is described in the moving-boundary (growth) frame by the pair of coupled equations

$$\partial_t u = a - bu - 4\frac{uv}{1+u^2} - \phi + \partial_x^2 u,$$

$$\partial_t v = \sigma\left(bu - \frac{uv}{1+u^2} + \phi + d\partial_x^2 v\right), \tag{11}$$

or in the flow frame

$$\partial_\tau u = a - bu - 4\frac{uv}{1+u^2} - \phi + \partial_\xi^2 u - V\partial_\xi u,$$

$$\partial_\tau v = \sigma\left(bu - \frac{uv}{1+u^2} + \phi + d\partial_\xi^2 v\right) - V\partial_\xi v. \tag{12}$$

Here u and v are the dimensionless concentrations of activator (iodide) and inhibitor (chlorite), respectively; a, b, d, and

σ are control parameters; and $\phi=\phi(x,t)$ is a dimensionless variable representing the intensity of illumination of the medium. The effective ratio of inhibitor and activator diffusion coefficients is given by σd. We choose parameter values that mimic the conditions of recent experiments [15], namely, $a=22$, $b=1.3$, $d=1.07$, $\sigma=8.5$, and $V=20$. In the experiments, the growing medium, the moving boundary, and the driven boundary conditions are all created by means of variations in the illumination—a video projector creates a boundary moving at 0.42 ± 0.08 mm/min. Specifically, we set

$$\phi=\phi_{\min}=2 \quad (x<Vt),$$

$$\phi=\phi_0+\phi_1\cos\omega_D t=3+\cos\omega_D t \quad (x>Vt). \tag{13}$$

The minimum illumination $\phi_{\min}$ corresponds to the low ambient illumination (approximately 10^{-3} W/cm^2) that is present in the experiments. The system undergoes a Hopf bifurcation at $\phi\approx2.197$, so the conditions are such that in the region $x<Vt$ free oscillations are allowed, while in the rest of the space they are (mostly) suppressed and the concentrations instead oscillate with time as a result of the oscillating light intensity. The former region forms the growing medium, while the latter sets the boundary condition at the border of the growing region. In the region where $\phi=2$, the homogeneous steady state is subjected to both Turing and Hopf instabilities.

Numerical solutions of the dispersion relation for small-amplitude waves [Eq. (10)] are plotted in Fig. 2. As discussed in [22], there are two physically relevant solutions for each value of ω_F. We plot the growth rates Im k_F and the phase velocities $c_M=\omega_M/\mathrm{Re}\,k_M$ in the moving-boundary frame. One of the two solutions has a positive growth rate for $0.20<\omega_F<1.75$ and corresponds to FDO modes, while the other grows for $4.21<\omega_F<6.60$, corresponding to the Turing modes. Note that the FDO modes occur for frequencies near the natural oscillation frequency ω_0, and their phase velocity has a pole at $\omega_F/\omega_0=1$. The Turing modes, on the other hand, have zero phase velocity as they are stationary patterns with respect to the medium. Their frequencies are directly proportional (with a factor of V) to the wavelengths of unstable Turing modes, thus obeying the geometrical relationship of Eq. (9). The dispersion relation describes the behavior of small-amplitude perturbations to the unstable equilibrium and, to a first approximation, we expect the growing perturbations to lead to saturated finite-amplitude waves at the same frequencies. Perturbations at other frequencies are expected to be damped.

IV. NUMERICAL RESULTS: RESONANT DRIVING OF FDO WAVES AND TURING PATTERNS

Recent experiments with the CDIMA reaction have demonstrated the excitation of both FDO and Turing modes by means of an oscillatory perturbation at a moving boundary [15]. Rather than a small perturbation of the unstable fixed point, the driving is achieved by means of the strongly varying illumination [Eq. (13)]. (We will discuss the significance of this difference below.) We have simulated these experiments by numerically solving model (11) using an explicit

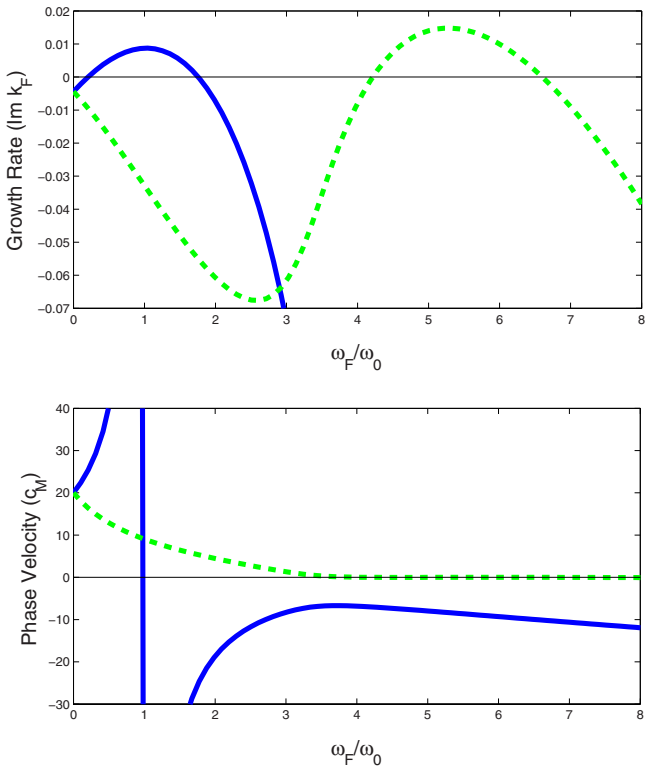

FIG. 2. (Color online) Solutions of the dispersion relations for small-amplitude waves. Each solution branch has positive growth rate for a different range of frequencies. The growing modes on the solid curve (blue online) correspond to FDO modes. Their phase velocity has a pole near the natural oscillation frequency. The growing modes of the other solution branch (dotted curves, green online) are Turing modes. Their phase velocity is zero in the moving-boundary (M) frame of reference.

second-order algorithm with spatial step $\Delta x=0.2$ and time step $\Delta t=0.01$. An example with driving frequency $\omega_D=0.8\omega_0$ is shown in Fig. 3. The gray levels in this and the following space-time plots represent the variable u as a function of space and time. The frequency $0.8\omega_0$ is within the range where linear analysis predicts FDO modes (see Fig. 2). Traveling waves are indeed generated and their frequency f_F, as measured at a constant distance behind the boundary (along the dotted white line in the figure), is equal to the driving frequency, in agreement with Eq. (8).

As in all of the simulated space-time plots shown, two main regions can be distinguished in this plot, separated by a diagonal that marks the trajectory of the moving boundary. To the right of this diagonal is the *driving region* in which the variable illumination is imposed, and the chemical concentrations respond directly to the changes in illumination. The resulting forced oscillations (due mainly to the illumination and not to self-oscillation) appear as horizontal bands on this region of the plot. To the left of the moving boundary is the *active* or *pattern-forming region* where the chemical system oscillates freely at a constant illumination and patterns are formed in response to the boundary condition. The active region can further be subdivided into a *transient region* close to the boundary—where waves propagate unevenly, have a zigzag appearance, and may display various forms of

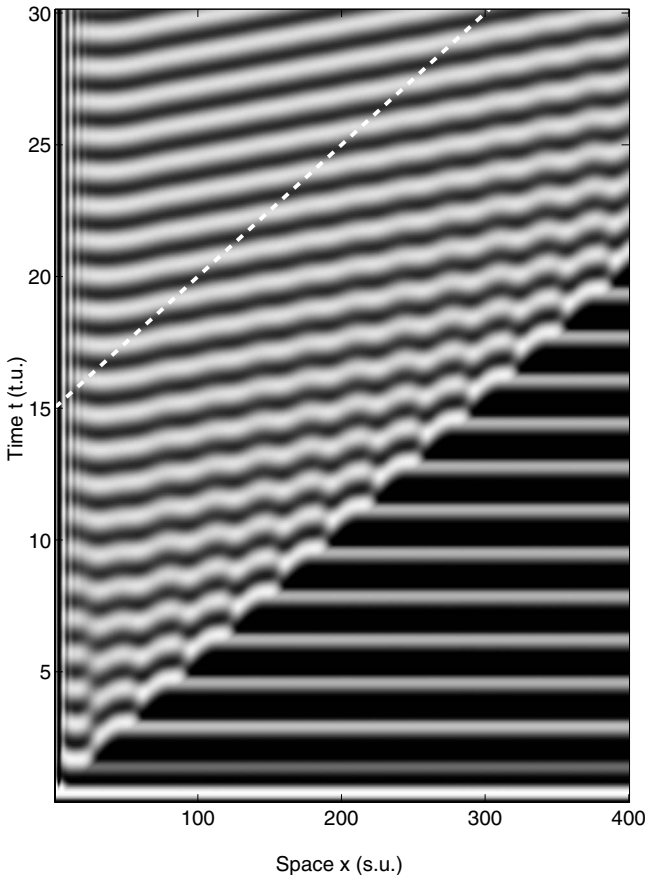

FIG. 3. Simple 1:1 driving of FDO waves by the oscillating boundary. The driving frequency is $\omega_D/\omega_0=0.8$. A diagonal line across the space-time plot marks the moving boundary between the driving and the active regions. A dotted white line shows the trajectory of a fiducial point following at a constant distance behind the moving boundary. ω_F is defined as the wave frequency measured along this line.

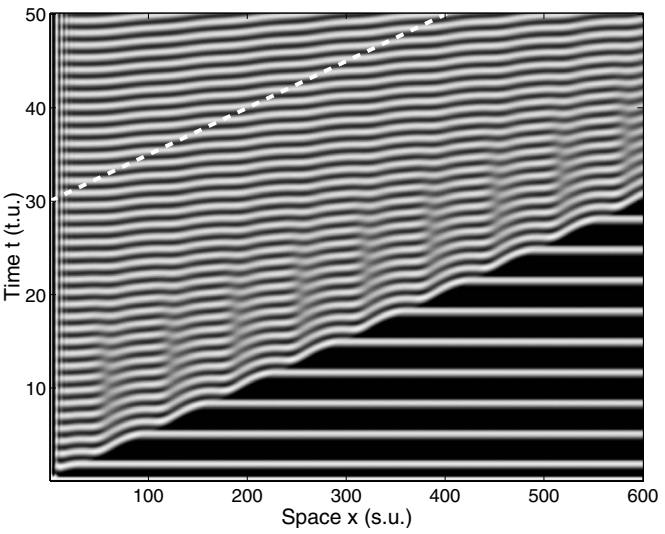

FIG. 4. Example of a 2:1 resonance of the FDO mode, with $\omega_D/\omega_0=0.4$. Transient waves excited by the boundary undergo dislocations. Far behind the moving smoothly traveling phase waves appear. Their frequency, measured at a position a constant distance behind the moving boundary (i.e., along the dotted white line shown in the plot) is twice the driving frequency supplied by the boundary.

complex transient behavior that will be discussed below—and an *asymptotic region* farther from the boundary, in which the waves are smooth and have frequencies and wavelengths obeying kinematic relations. There is also a *boundary layer* where the patterns are under the influence of the fixed $x=0$ boundary (at the opposite end of the medium from the growth boundary). Boundary layer effects were noted in the experimental results [15]. For the current work, we are less interested in the boundary layer than in the transient and the asymptotic regions. In most cases, the boundary layer has a fixed thickness. If the medium stops growing after reaching a maximum length $L_{\max}$ as it generally does in experiments, then another boundary layer may form at the now fixed right boundary $x=L_{\max}$ while patterns that were formed under the moving boundary's influence persist in the middle of the active region.

Figure 5 shows a simulation with driving frequency $\omega_D/\omega_0=5$. This frequency is in the middle of the band in which Turing patterns are predicted, and one in fact finds asymptotic waves that are stationary with respect to the medium (a characteristic of Turing patterns). Further investigation shows that the activator and the inhibitor concentrations are 180° out of phase, as expected for Turing patterns. The wavelength of these Turing waves is given by $\lambda=VT_D$ in agreement with Eq. (9). In other words, each cycle of the driving signal generates one wave as the boundary moves. This can be verified by a close inspection of the space-time plot. The Turing patterns grow slowly and only reach their full amplitude at a significant distance behind the advancing boundary (or at a significant time after the boundary has passed). Initially, close to the boundary, a transient FDO-type wave with $\omega_F=0$ dominates. This FDO wave is excited by the strong zero-frequency component in the driving signal as we discuss below. However, as predicted by the dispersion relation solutions (Fig. 2), the FDO wave with $\omega_F=0$ is damped and it decays as the Turing mode begins to emerge. Each cycle of the driving oscillation produces a small bump in the first wave front of the transient FDO wave, and each of these bumps eventually develops into a single Turing wave.

Both of the above examples (Figs. 3 and 5) show wave patterns whose (flow-frame) frequency is equal to the driving frequency, the standard situation for waves driven convectively by the upstream boundary. In contrast, Fig. 4 shows a simulation done at $\omega_D/\omega_0=0.4$. As in Fig. 3, FDO-type waves emerge in the asymptotic region behind the boundary. In this case, however, the waves have frequency $\omega_F=0.8\omega_0=2\omega_D$ or *twice* the driving frequency. The other parameters of these waves (wavelength, phase velocity, and growth-frame frequency ω_M) obey the usual geometrical or kinematic relations, just as if they had been generated by a driving signal with $\omega_D/\omega_0=0.8$. Examining the space-time plot, one can see that in the transient region behind the moving boundary, the initially generated phase fronts undergo

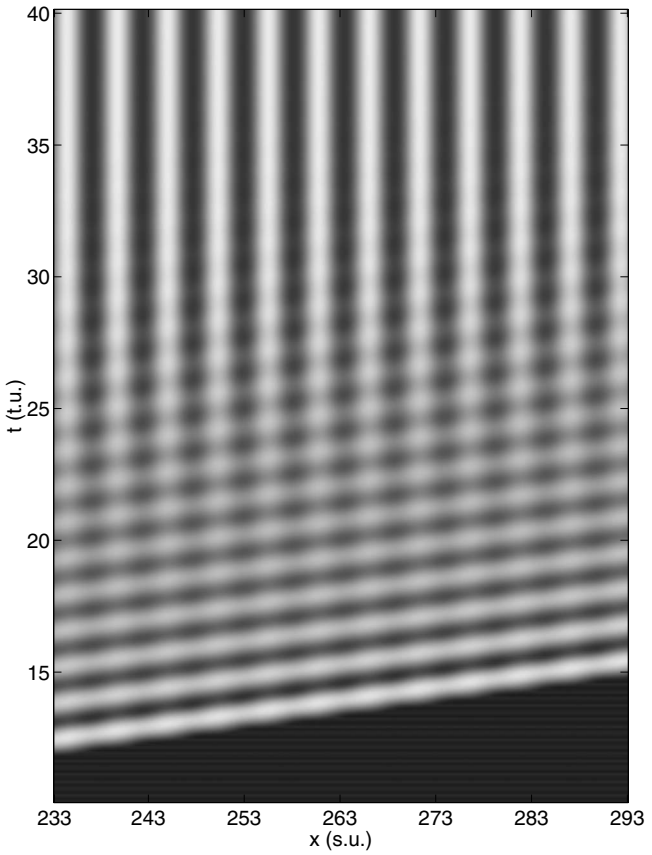

FIG. 5. Space-time diagram showing the excitation of Turing patterns with wavelength controlled by the boundary forcing frequency $\omega_D/\omega_0=5.0$. Immediately behind the boundary, there are transient FDO waves, due to the strong zero-frequency component of the driving. The Turing patterns emerge slowly as the zero-frequency waves decay. (In this and the following figure, we show only a segment of the system, far from the $x=0$ boundary layer.)

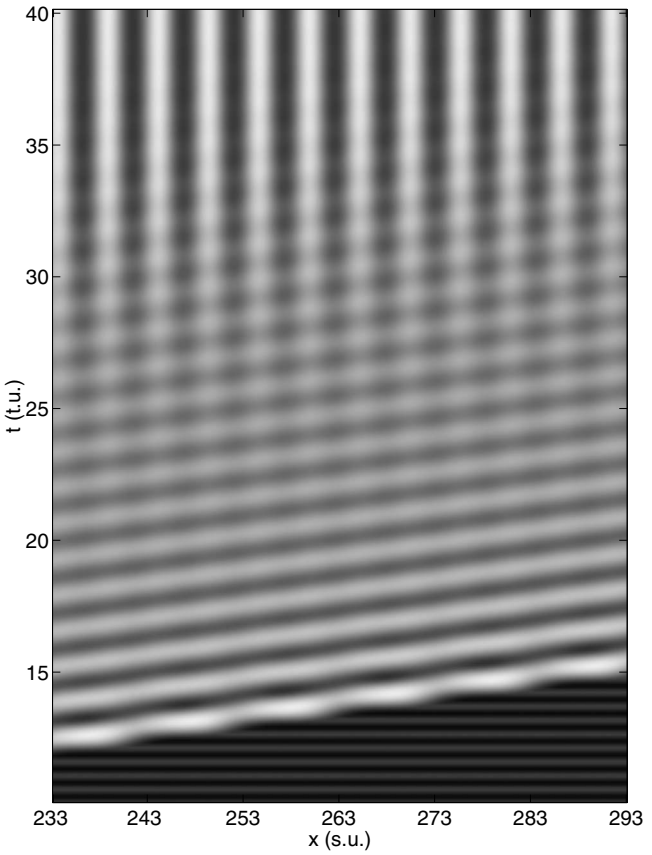

FIG. 6. 2:1 resonant driving of a Turing pattern. The driving frequency is exactly half that of Fig. 5 ($\omega_D/\omega_0=2.5$), but Turing patterns of the same wavelength are produced. One can see that, in this case, each oscillation of the boundary condition produces two Turing waves rather than one. As before, the Turing patterns take time to emerge from the transient FDO waves.

dislocations,[3] resulting in waves at the new frequency.

A harmonic resonance can also be seen in the Turing modes, as in Fig. 6. Here the driving frequency is $\omega_D/\omega_0=2.5$, where the linear dispersion relation predicts no undamped modes. However, what we find is Turing patterns with the same wavelength as in Fig. 5, even though the driving frequency is half as large. In this case, for each cycle of the driving signal the moving boundary deposits two Turing waves rather than one. Examining the space-time plot, it appears that as before there is an $\omega_F=0$ FDO wave that dominates immediately behind the boundary. The oscillatory response of the driving region ahead of the boundary is again a rather small perturbation superimposed on the strong zero-frequency component. As in the other example, each oscillation of the driving signal produces one slight but clearly observable bulge in the first downstream FDO phase front. These bulges at first seem to decay; but with more time, the FDO wave damps and each of the bulges ultimately splits into two Turing waves, which in turn reach full amplitude as the FDO wave disappears.

What these four examples (Figs. 3–6) have in common is that the oscillatory driving of the upstream driving region (in front of the boundary) gives rise to waves which asymptotically emerge at a sufficient distance downstream (or behind the boundary) and whose frequency, *as reckoned in the flow frame or at a constant distance behind the boundary*, is an integer multiple of the driving frequency $\omega_F=n\omega_D$, where $n=1,2,3\ldots$ The examples shown above are in ratios of 1:1 or 2:1. The emerging asymptotic waves may be either Turing or FDO, and they generally emerge downstream from a complex transient region.

In other numerical integrations, we have observed similar resonances at higher-integer multiples of the driving frequency as well. Our results are summarized in Figs. 7 and 8 for the FDO and the Turing modes, respectively. In Fig. 7, we plot the characteristics of the asymptotic FDO waves as functions of the driving frequency. The ratio ω_F/ω_D of wave frequency to driving frequency shows a staircase jumping discontinuously from one integer to another. We emphasize that the waves that eventually emerge have frequencies ω_F within the range predicted by the linear dispersion relation and obey the kinematic relations. Likewise for the Turing

[3]We use the word "dislocation" by analogy with an edge dislocation in a crystal structure, based on how the phenomenon appears in the space-time diagram, with wave fronts looking like crystal planes with a dislocation.

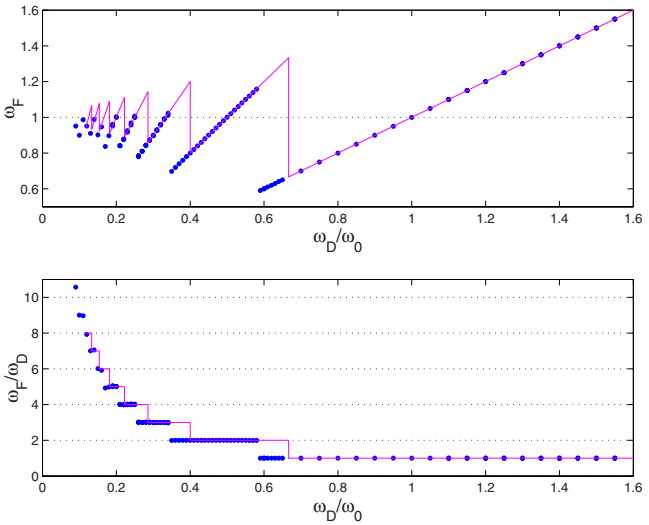

FIG. 7. (Color online) Resonance staircase for the FDO mode. The ratio of the (flow-frame) frequency of the asymptotic wave to the driving frequency takes a series of integer values n, as shown in the lower panel. The nth plateau covers a range of driving frequencies that includes ω_0/n. The points (blue online) show the numerical measurements, while the solid lines (pink online) show the "theoretical" staircase described in Sec. V.

resonances (Fig. 8), the waves that finally emerge have wavelengths and frequencies within the range predicted by linear analysis, even when the driving frequency itself is outside of that range.

A difference between the FDO and the Turing cases is that we find some frequencies where Turing modes emerge that

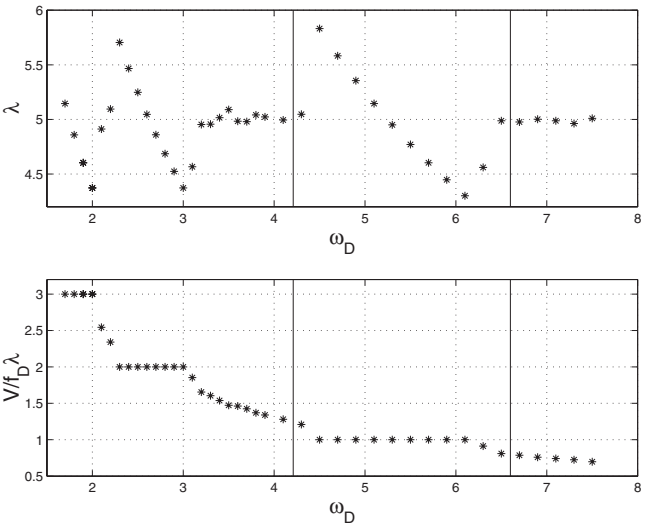

FIG. 8. Resonant excitation of Turing waves. The vertical lines show the limits of the frequency range in which the linear dispersion relation predicts growing Turing modes. The wavelength (top panel) always takes values within the Turing-unstable range of the medium. The dimensionless ratio $V/f_D\lambda = Vk/\omega_D$ takes integer values at resonances. Unlike the FDO case, however, there are frequencies at which Turing modes occur that are not locked to the driving frequency. For these frequencies the ratio has noninteger values and the wavelength is near the free-running (most unstable) Turing wavelength.

are not locked to the driving frequency, but instead are near the "free-running" (i.e., most unstable) Turing wavelength. As a result of this, the jumps between steps of the resonance staircase are not discontinuous as in Fig. 7 but instead separated by smooth transitions.

As a general rule, we observed that, the higher the resonance ratio ω_F/ω_D, the larger the transient region and the longer it took the FDO waves to settle into a smoothly periodic form. Some numerical fluctuations in the measured wavelengths resulted from making measurements in a region where the asymptotic wave form was not fully settled. Such fluctuations are noticeable in Fig. 7 and generally increase with higher ratios. We found no evidence of resonances with ω_F/ω_D taking other rational values such as 1/3, 3/2, etc.; only integer values were observed.

V. TOPOLOGICAL AND GEOMETRICAL INTERPRETATION OF RESONANCE MECHANISM

In this section we offer a general qualitative explanation of resonances, wave dislocations, and related phenomena in FDO waves. We interpret the mechanism of the breakup and the reformation of waves as a type of constrained synchronization phenomenon in the extended medium.

We begin with a closer look at the space-time plots of Figs. 3 and 4, focusing on the transient region a short distance behind the boundary. In both cases, the wave fronts (black or white stripes) in this region have a zigzag appearance: phase fronts speed up and slow down rather than moving uniformly as they do farther away from the boundary. In the case of Fig. 3, the average slope is evidently the same as that of the smoother waves farther downstream. The zigzags gradually become smoothed out as the waves propagate downstream. Such zigzags or "jumping" waves were noted previously in FDO experiments [23] when the wave form used for driving does not conform to the limit cycle of the freely running chemical oscillator. Depending on details of the system, these zigzags may persist much further downstream. In general, stronger diffusion tends to smooth the zigzags more rapidly than weak diffusion, as we show in an example below. In the second case (Fig. 4), the wave fronts immediately behind the boundary have qualitatively a similar zigzag appearance as in Fig. 3, although their average slope (corresponding to the inverse phase velocity) is steeper than that of the wave fronts in the first example. Unlike the first case, however, these zigzags do not grow smoother with downstream distance, but instead they become more uneven until a dislocation or a wave-front splitting occurs. Following the white stripes in Fig. 4 along a vertical line, one can see that at a certain point, a segment of each stripe disconnects from a segment of the stripe to its left and reconnects to a stripe segment immediately below it. The dislocation results in reattached wave fronts with a less steep average slope (thus, a faster phase velocity) than the initial ones. The unevennesses in the newly reformed waves decay with downstream distance, leading asymptotically to smoothly propagating waves with a frequency (in the flow frame) twice the driving frequency. To summarize, qualitatively similar zigzag wave fronts appear initially in both cases, but in one case

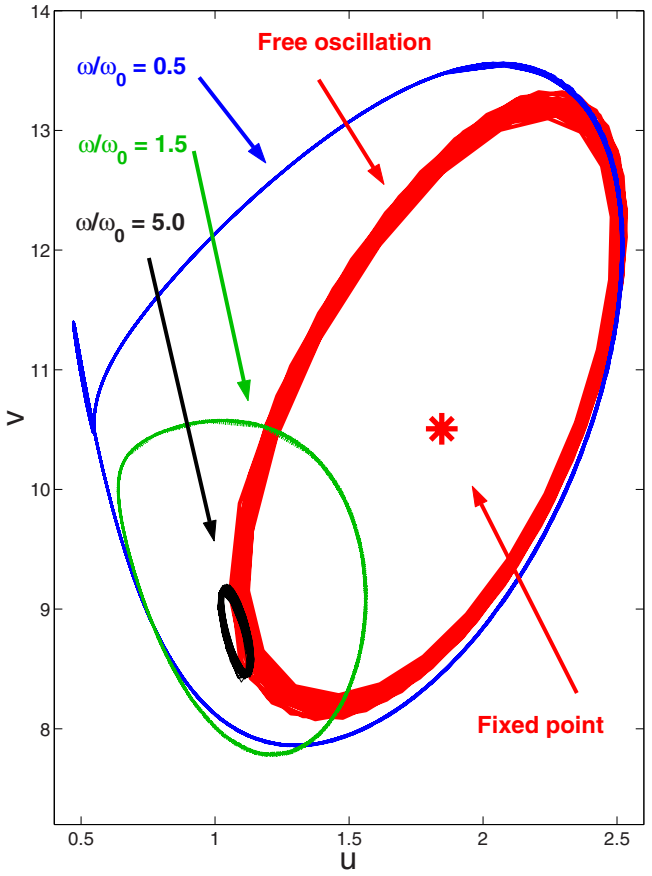

FIG. 9. (Color online) Phase-space trajectories (u vs v) of the response of the CDIMA model to the sinusoidally varying illumination Eq. (13) at several different frequencies. For comparison, the unstable fixed point and the limit cycle of the freely running system for $\phi=\phi_{\min}=2$ are shown on the same axes. The driving cycle is clearly not congruent with the freely running limit cycle. In all cases, there is a significant average displacement to one side of the fixed point (i.e., a dc or zero-frequency component). For higher frequencies, the oscillatory response is quite weak compared to the dc component.

the zigzags gradually damp, while in the other they grow until they trigger a wave-front dislocation. We will argue that a topological constraint lies at the root of this difference.

A. Driving signal shape and marking of periodic positions

The transient behavior of oscillations near the boundary is surely affected by the driving signal, which is not congruent with the system's natural limit cycle. Figure 9 shows the two-dimensional phase-space trajectories of the Lengyel-Epstein model's response to varying illumination of form (13) at several different frequencies. These curves model the imposed oscillations that occur in the driving region to the right (ahead) of the moving boundary and that in turn supply the driving signal to the boundary of the active region. The limit cycle of the freely oscillating system with $\phi=2$ is shown on the same axes. In all cases the chemical driving signal differs significantly from the freely running limit cycle, nor can it in any sense be considered a small perturbation of the fixed point (as is implicitly assumed in the linear analysis). In all cases there is a significant sideway displacement on average, which can be viewed as a zero-frequency or a dc component within the driving signal. This is unsurprising given that the average illumination in the driving region is higher than in the active pattern-forming region. With increasing frequency, the amplitude of the driving oscillation shrinks in comparison to the dc component.

Viewing the driving as a superposition of signals with frequencies 0 and ω_D suggests that the response can be approximated by two superposed FDO waves of form (3), both assumed to be in the kinematic limit, so that $\omega_M=\omega_0$. This view is consistent with the appearance of the transient region in the space-time plots of Figs. 3–6. One wave, resulting from the dc component of the driving, has $\omega_F=0$ while the other has $\omega_F=\omega_D\neq 0$. Using Eqs. (4)–(6) we get for the two waves $k_{M0}=\omega_0/V$ and $k_{MD}=(\omega_0-\omega_D)/V$, respectively. The two waves, described in moving-boundary coordinates by the forms

$$\psi_0=\psi\left(\omega_0 t-\frac{\omega_0}{V}x\right),\quad \psi_{Osc}=\psi\left(\omega_0 t-\frac{\omega_0-\omega_D}{V}x\right), \tag{14}$$

interfere constructively (i.e., have the same phase) at the points $x=2\pi nV/\omega_D$, for integers n, independent of t. The addition of the dc component marks particular positions, imposing a spatial periodicity that is different from the wavelength of the traveling wave.

The marking of periodic positions occurs more generally with any driving cycle that differs from the limit cycle, because the deviations from the limit cycle are not equal on all parts of the cycle, and the chemical system at each position preserves the memory of deviations that occur in the particular part of the cycle where that element entered the active region. Keeping in mind that x and ξ are proportional to the time at which a particular element of the medium left the boundary, and the time elapsed since it left the boundary, respectively, we can see that two points at the same ξ but separated by $\Delta x=2\pi nV/\omega_D$ are equivalent, due to the periodicity imposed by the boundary condition. As a result, the space-time diagram of the chemical system can be split into cells of width $2\pi nV/\omega_D$ as illustrated in Fig. 10. Fluid elements (positions) within each cell are "marked" according to the phase of the driving cycle at the time each element left the boundary. The behavior of the system inside each cell is identical to each other cell up to a combined space and time translation.[4]

B. Phase kinematics and zigzags

In the kinematic limit of negligible diffusion, each point in the medium at a particular value of x can be considered as

[4]The requirement for the complete equivalence of cells is that the system is under no influences other than the periodic driving. The assumption therefore breaks down at boundary layers (such as near the fixed end of the medium opposite to the moving boundary) or in the presence of aperiodic noise.

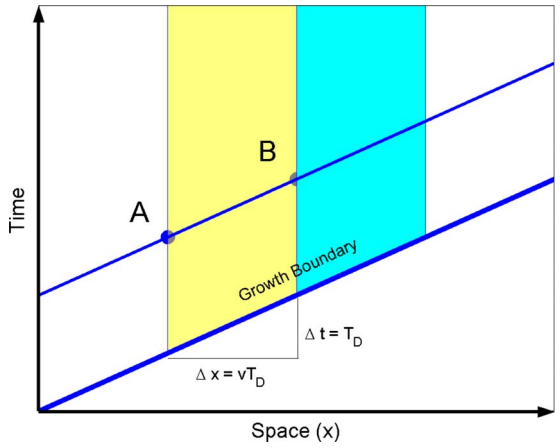

FIG. 10. (Color online) Dividing space-time into equivalent cells. Points A and B lie along a line of constant ξ and are separated by the width of one periodic cell, so they are equivalent in terms of the periodicity.

an independent oscillator whose initial condition is set when it enters the active region at time $t=x/V$. In this limit, oscillators at different positions do not interact. As a further simplification, suppose that, from its initial condition, each of these oscillators is quickly attracted to the limit cycle and subsequently runs along the limit cycle with some phase shift that depends on the initial condition and therefore on x. In other words, the phase-space vector $\mathbf{u}$ is given by

$$\mathbf{u}(x,t) = \bar{\mathbf{u}}(\omega_0 t + \delta(x)), \tag{15}$$

where $\bar{\mathbf{u}}(\omega_0 t)$ represents the limit cycle [periodic so that $\bar{\mathbf{u}}(\omega_0 t+2\pi)=\bar{\mathbf{u}}(\omega_0 t)$] and $\delta(x)$ is the position-dependent phase shift.

First, consider the simplest case where the boundary condition is stationary. In this case, each element enters the active region with the same initial condition, but there is a uniform phase shift gradient because they enter at different times. Considering two points separated by a distance Δx, the one with larger x (to the right in the moving-boundary frame) enters the active region $\Delta t=\Delta x/V$ later and therefore its phase is retarded by the corresponding amount

$$\Delta\delta = -2\pi\frac{\Delta t}{T_0} = -\omega_0\frac{\Delta x}{V}. \tag{16}$$

The phase fronts [loci where $\omega_0 t+\delta(x)=\text{const}$] on the space-time diagram have a constant slope $1/V$: they are parallel to the trajectory of the boundary.

Now, suppose that, instead of being static, the boundary condition is oscillating at frequency ω_D, approximately but not exactly following the (sped up or slowed down) limit cycle. In this case, the phase advances by 2π for each driving cycle. Points separated by $\Delta x=VT=2\pi V/\omega_D$ enter the active medium at the same initial conditions although at different times. The phase advance of 2π that occurs between two such points is added on top of the retardation caused by the motion of the boundary and the fact that the second point enters later. The net phase difference then is

$$\Delta\delta = 2\pi - \omega_0\frac{\Delta x}{V} = 2\pi\left(1-\frac{\omega_0}{\omega_D}\right). \tag{17}$$

This means that the *average* phase shift gradient is

$$\frac{\Delta\delta}{\Delta x} = \frac{\omega_D-\omega_0}{V}. \tag{18}$$

Thanks to deviations between the driving cycle and the limit cycle, however, this gradient need not be uniform. It must be periodic over the period $\Delta x=2\pi V/\omega_D$, but within this period it may be steeper at some positions x than at others. The same is true for the phase fronts, resulting in zigzags as in the transient regions of Figs. 3 and 4. One can verify in those pictures that bands of x values occur periodically where all phase fronts move faster, alternating with bands where they are slower. Portions of the driving cycle that is slow compared to the limit cycle leave their imprints at values of x where the slopes of the phase fronts are nearly the same as the boundary, because in these places the phase gradient is mainly due to the motion of the boundary.

We note that qualitatively the same effect (uneven phase gradients and unevenly moving phase fronts) can occur in the case where the boundary condition is stationary ($\omega_D=0$) but the boundary does not move uniformly. There is again an average phase gradient (hence an average slope of the phase fronts) determined by the average boundary velocity, but each portion of the medium preserves a memory of the speed of the boundary at the time when the portion entered the active region. When the boundary moved quickly, the phase fronts move quickly. In experiments with growing media and a sinusoidally modulated velocity, FDO waves were generated with (flow-frame) frequency equal to the velocity modulation frequency, while in numerical studies of a flow system, a series of integer resonances was found. The reasoning here suggests strongly that the underlying mechanism is the same as in the resonant driving described here, involving the same type of breakup of zigzag phase fronts.

C. Role of diffusion

The role of diffusion can be appreciated most easily in the moving-boundary frame, where it is uncomplicated by advection. Since it smooths local nonuniformities, diffusion has a synchronizing effect.

Both the smoothing of zigzag or jumping waves and the dislocations of phase fronts can be interpreted as forms of partial synchronization. The former smooths abrupt phase shifts in favor of more gradual ones, while the latter leads invariably to waves with ω_F closer to ω_0 than the original transient ones, and thus to smaller average phase gradients.

Confirming the importance of diffusion in both of these effects, in Fig. 11 we plot additional space-time plots for $\omega_D/\omega_0=0.8$ and 0.4. The conditions are identical to those of Figs. 3 and 4 except that the diffusion coefficients of both activator and inhibitor are reduced by a factor of 10. Not only do the transient zigzags of the phase fronts persist much longer, but the breakup into higher-frequency lower-slope waves fails to occur in the case $\omega_D/\omega_0=0.4$.

Having noted that the smoothing of jumping waves reduces the largest phase gradients and that the resonant wave

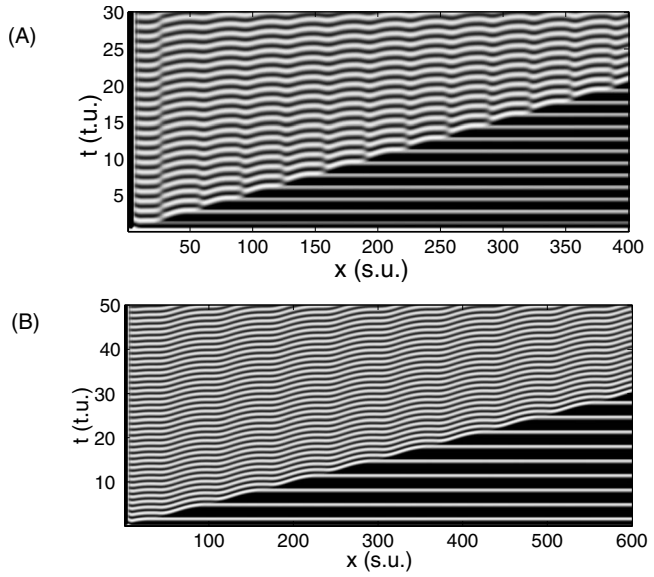

FIG. 11. Space-time plots for conditions identical to (A) Fig. 3 and (B) Fig. 4 except that the diffusion coefficients are reduced by a factor of 10. The zigzag appearance of the transient waves is not smoothed out nearly as promptly, and the wave dislocations fail to occur in the case with $\omega_D/\omega_0=0.4$ [plot (B)].

breakup reduces the average phase gradient, we see, however, that in neither case phase gradients are eliminated entirely. The constraints imposed by the periodic boundary forcing prevent this, as the phase shift per periodic cell can only change by an integer. To see why, we can view the total phase shift $\Delta\delta$ across a cell (at constant t) as composed of two parts: one being the phase shift across the cell along a line of constant ξ, which is the phase shift imposed by the periodic driving, and another part due to the delay across the cell, which is a result of the boundary's motion. Because of the periodicity, the former must always be an integer.

In an abstract sense, the reasoning that applies here is the same as in the theory of topological defects familiar to field theorists and condensed-matter physicists [19]. A useful point of view is to parametrize space-time using the two coordinates x and ξ and to consider $\mathbf{u}(x,\xi)$ as a function of x that evolves with changes in ξ. If one considers $\mathbf{u}(x)$ along a line of constant ξ, this function is periodic with a period of $2\pi V/\omega_D$. [It is worth noting that, to the extent that the boundary forcing is strictly periodic, this periodicity in x is also a strict periodicity, originating in a constraint imposed by the boundary conditions. The periodicity in terms of t (or ξ), by contrast, is of dynamical origin, and holds only when transients have decayed.] This means that points separated by $2\pi V/\omega_D$ are effectively topologically identified, and if $\mathbf{u}$ is confined to the limit cycle then the function $\mathbf{u}(x)$ is effectively a mapping from S_1, the unit circle, onto S_1. Such mappings are characterized by an invariant integer *winding number* which cannot be changed by continuous deformations of the map. The winding number in this case means the number of times $\mathbf{u}$ winds around the limit cycle within each cell. The configuration $\mathbf{u}(x)$ can evolve to one with a different integer winding number, but only by departing from the limit cycle and passing through the unstable fixed point at some point in space-time. [As put differently, this means that at some point the phase angle δ is undefined and $\mathbf{u}(x)$ temporarily ceases to be a mapping from S_1 to S_1.] In order for this to happen, a dynamical barrier (the repulsiveness of the unstable fixed point and the attractiveness of the limit cycle) must be crossed.

By crossing this barrier and changing the winding number, it is sometimes possible to reduce the overall phase gradient. Specifically, if the phase shift $\Delta\delta$ across a cell along a line of constant ξ changes from 2π (the initial value it has due to the driving), to some other integer multiple $2\pi n$, then the *physical* phase shift across the cell (i.e., along a line of constant t rather than constant ξ) becomes

$$\Delta\delta = 2\pi n - \omega_0\frac{\Delta x}{V} = 2\pi\left(n - \frac{\omega_0}{\omega_D}\right), \tag{19}$$

so that the average gradient is

$$\frac{\Delta\delta}{\Delta x} = \frac{n\omega_D - \omega_0}{V}. \tag{20}$$

The new phase shift (19) includes both the phase shift at constant ξ and the additional contribution from the phase delay induced by the motion of the boundary. Since the rate of change in phase shift along a line of constant ξ is what is being measured by the frequency ω_F, the resonance mechanism in which ω_F changes to a multiple of its original value is precisely such a change as we are describing. This change reduces the average phase gradient if

$$|n\omega_D - \omega_0| < |\omega_D - \omega_0|. \tag{21}$$

For example, if $\omega_D=0.4\omega_0$, then we have $|2\omega_D-\omega_0|=0.2\omega_0 < 0.6\omega_0=|\omega_D-\omega_0|$. By *increasing* the phase gradient along a line of constant ξ, therefore, it is possible to *decrease* the gradient along a line of constant x, and it is the latter gradient that is acted on by diffusion.

Condition (21) can be interpreted as a condition that predicts when one may find an $n:1$ FDO resonance, since it describes when a multiplication of the flow-frame frequency can lead to a reduction in the physical phase gradient. This gives a series of thresholds leading to the staircase plotted as a solid line in Fig. 7. Specifically, each threshold [from the nth to the $(n+1)$th resonance] occurs at the frequency ω_D for which

$$|n\omega_D - \omega_0| = |(n+1)\omega_D - \omega_0|. \tag{22}$$

Evidently, the actual thresholds found in the numerical simulations fall at lower values of ω_D than the ones predicted by Eq. (22). This can be understood by recalling that a change in winding number requires the surmounting of a dynamical barrier. The barrier becomes more likely to be overcome as the phase gradients increase (i.e., the system is driven farther from its preferred state of synchronous oscillation) and/or as diffusion coefficients increase.

In the analogy with topological defects [19], diffusion plays the same role as gradient terms whose tendency is to make the configuration of dynamical variables as smooth as possible, while the chemical dynamics (the repulsion from the fixed point and attraction to the limit cycle) play a role

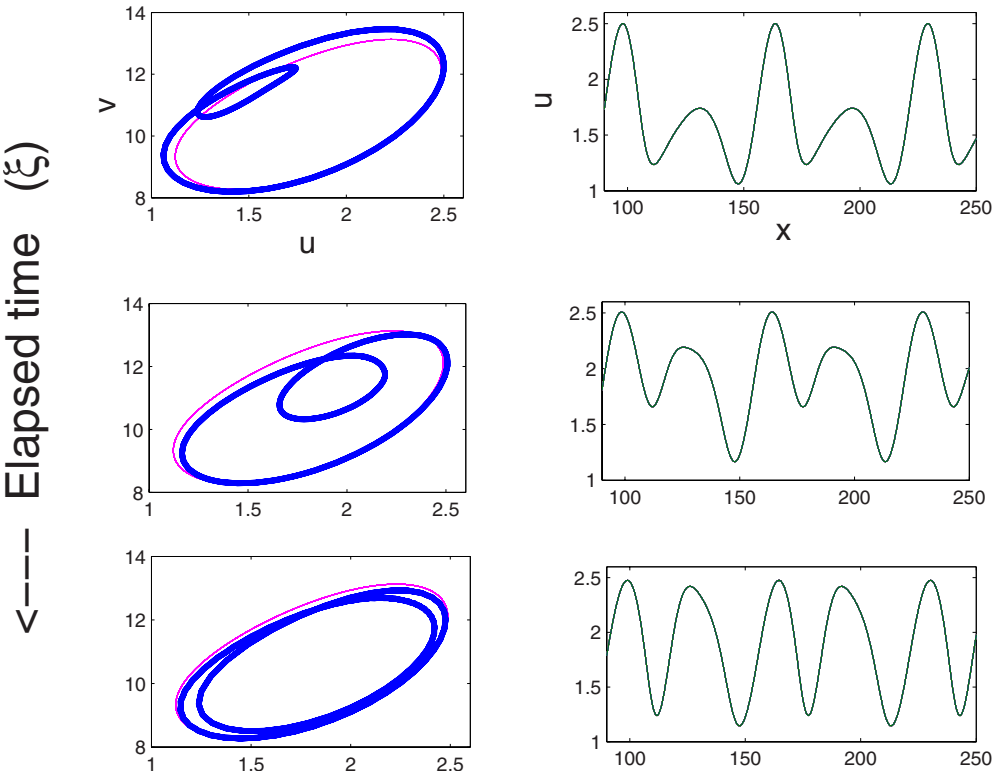

FIG. 12. (Color online) Profiles of phase-space variables along lines of constant ξ (i.e., at constant distance behind the moving boundary with x varying) for a case with 2:1 resonance. The profiles evolve in a manner reminiscent of an inverse period-doubling transition, adding an extra loop around the limit cycle. For reference, the limit cycle of the batch system is shown as a thin curve (pink online) in the phase-space plots. The original waves split into waves of twice the original frequency. Successive plots are taken approximately at multiples of the natural oscillation period, i.e., $\xi=nVT_0$.

analogous to the Higgs potential, providing a barrier against the unwinding of phase gradients. According to this interpretation, strengthening the relative effect of diffusion should move the observed thresholds closer to the ones predicted by Eq. (21) by making it easier for diffusion effects to overcome the barrier. The finding that 2:1 resonance failed to occur when the diffusion coefficients were lowered (Fig. 11) is consistent with this idea.

The process of changing the winding number can be followed explicitly in Fig. 12, which shows plots of **u** as a function of x along a series of lines of constant ξ, i.e., at points moving a constant distance behind the boundary. These phase-space profiles are based on the same data as the space-time plot of Fig. 4. Initially, this phase-space profile winds once around the limit cycle in each unit cell of x displacement. But as ξ increases (as one moves farther behind the boundary), a secondary loop develops along the original phase-space loop, which grows until it becomes a second full loop around the limit cycle. The progression is analogous to the inverse of a period-doubling transition in a temporal oscillator. In contrast, Fig. 13 shows the corresponding phase-space profiles along cross sections of the space-time diagram (Fig. 3), in which case the doubling fails to occur. From these cross sections, one can see that the kink which is initially present on the phase-space loop fails to grow into a second full loop and instead becomes smoothed out.

To summarize, the smoothing of transient zigzags and the resonant wave breakup or dislocation mechanism can both be viewed as processes that smooth phase differences across space. In this sense, they are synchronization mechanisms. The dislocation, however, requires overcoming a dynamical barrier and, in general, neither process is capable of eliminating phase gradients completely due to the topological constraint that requires the phase winding number to change only by discrete units within each of the periodic cells imposed by the boundary driving.

D. Generality of resonance mechanism

The underlying pattern-forming instabilities of the medium in question (irrespective of boundary conditions and forcing) are Turing and Hopf instabilities. The FDO modes are consequences of the Hopf instability being driven by oscillatory boundary conditions. The uniformly oscillating mode ($k_M=k_F=0$) always has the highest growth rate among the FDO modes, and evidently a uniformly oscillating state is the preferred state of the medium, which is approached as closely as possible given the boundary conditions. Boundary conditions that drive the system at frequencies other than the natural frequency create phase gradients (i.e., traveling phase waves). If the frequency is far enough away from the natural frequency, and diffusion is strong enough, and if the periodicity imposed by the boundary conditions permits it, then the configuration may readjust itself to come closer to the preferred state of uniform oscillation. In general, the periodicity does not permit the unwinding of the entire phase gradient,

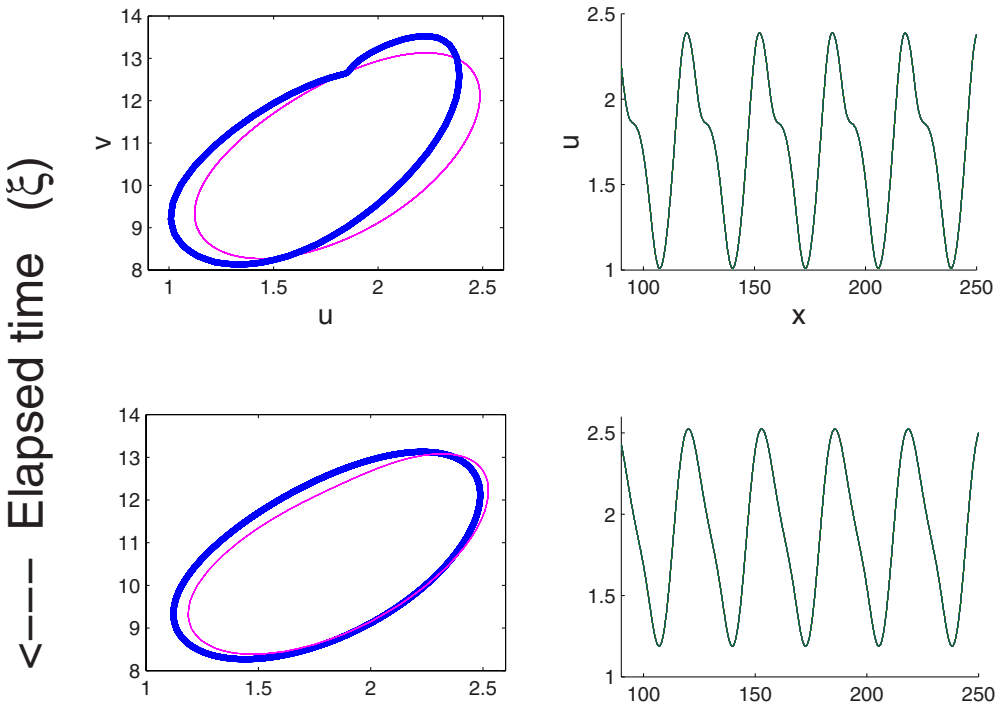

FIG. 13. (Color online) similar to Fig. 12, but at a higher driving frequency giving 1:1 resonance. Instead of expanding into a second full loop, the small kink on the phase-space profile becomes smoother.

but only a portion, because the phase winding number can only change by integer units within each periodic cell. This, then, is the essence of a quite general mechanism. Something analogous is recognizable in the results of simulations in which the flow velocity is modulated [16].

The details of the breakup mechanism can vary within this framework. As an example, the space-time plot in Fig. 14 shows a simulation of the same CDIMA medium driven at the boundary by a harmonic perturbation of the unstable fixed point instead of by the varying illumination. The boundary condition is

$$\begin{pmatrix} u \\ v \end{pmatrix}_{\xi=0} = \begin{pmatrix} u_0 + 0.15 \cos \omega_D \tau \\ v_0 + 0.15 \sin \omega_D \tau \end{pmatrix}, \tag{23}$$

where $\omega_D = 0.3\omega_0$ and the unstable fixed point is (u_0, v_0). In this form of driving, chemical concentrations are manipulated directly rather than via the illumination. FDO waves at the driving frequency grow slowly, eventually developing an instability which leads to their breakup and reformation into waves with $\omega_F = 3\omega_D$. In this case, the reformation happens via an intermediate step, where Turing-like stripes begin to form at each dislocation, and then disappear again with the growth of the reformed FDO wave. The addition of a small zero-frequency component to this harmonic perturbation was found to accelerate the breakup as one would expect based on the discussion above in Sec. V A, whereas in the case with driving by illumination at the boundary (where the zero-frequency component is much stronger) the breakup is even more prompt and occurs without the intermediate stage of Turing stripes.

In the case of the driving of the Turing instability, the most unstable wave number for Turing patterns is in the middle of the range of unstable wave numbers, and this gives the preferred wavelength for Turing patterns. Analogously to the FDO case, the boundary conditions can drive Turing patterns away from this preferred wavelength, but if the imposed wavelength is too far from the preferred value then the

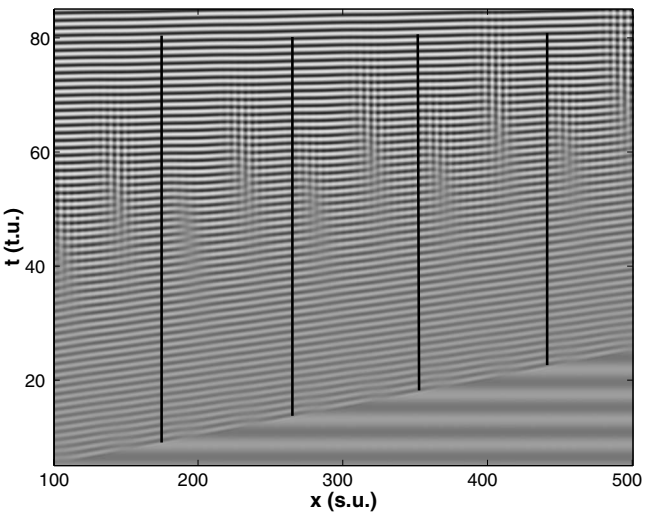

FIG. 14. Growth and breakup of FDO waves driven by a harmonic perturbation of the fixed point [Eq. (23)] instead of by illumination. The driving frequency is $\omega_D = \omega_0/3$, resulting in a 3:1 resonance. The vertical lines are guides to the eye illustrating the spatial periodicity (cells) imposed by the boundary oscillation. Since this is a 3:1 resonance, there are two dislocation events per cell, rather than one as in the 2:1 case. In this case each dislocation is accompanied by the temporary appearance and subsequent disappearance of Turing-like waves.

imposed patterns break down, either by doubling or tripling the wave number (integer resonance) or by some other adjustment resulting in new waves near the preferred wavelength. A key difference between the FDO and the Turing cases is that the preferred wave number for FDO is zero, while for the Turing patterns it is nonzero. Turing resonances will be studied more fully in another publication.

VI. CONCLUSIONS

We studied the selection of Turing patterns and FDO waves by oscillatory forcing at a moving boundary. Whereas previous discussions of patterns formed by driving at a moving or inflow boundary have assumed either that the boundary condition was stationary or that an oscillatory forcing would lead to waves at the same frequency as the forcing, in this case we examined cases where the frequency of the waves produced is an integer multiple of the forcing frequency.

It is important to keep in mind that the frequencies (as measured in the fixed-boundary frame) of all of the asymptotic wave patterns fall within the ranges for which the linear dispersion relations predict either FDO or Turing patterns. The available asymptotic waves are determined by the medium itself and are based on the underlying Hopf and Turing instabilities of the medium. The role of forcing at the boundary is simply to excite one or another of the competing wave patterns in the medium. As noted in [15], these patterns can be quite stable once excited—they maintain themselves after losing diffusive contact with the boundary and resist encroachment by boundary layers after the boundary stops moving. The current results show that a wave pattern can be excited by a more indirect mechanism than was previously considered. Boundary forcing may produce transient waves, which rearrange themselves via the splitting of wave fronts, resulting in waves at twice the frequency of the driving.

In general, for both the Turing and the FDO cases, we found that the asymptotic waves, if they have a frequency different from the driving frequency, have a frequency closer to some preferred frequency for that type of wave. In the case of FDO, that preferred frequency is the natural oscillation frequency of the underlying chemical system, and the preferred pattern is a uniform synchronous oscillation. The preferred Turing pattern, on the other hand, has a wavelength corresponding to the most unstable Turing mode. Under the right conditions, a transient wave pattern may split up so as to approach the preferred pattern more closely. The possibility of this happening is constrained by topological constraints imposed by the boundary conditions.

Diffusion is essential to the resonance mechanisms we consider. The resonant breakup of waves does not always occur where it is topologically permitted, because the chemical dynamics (understood as the repulsiveness of the unstable fixed point and the attractiveness of the limit cycle) presents a dynamical barrier that must be overcome.

ACKNOWLEDGMENTS

This work was supported by the NSERC of Canada. A.P.M. acknowledges financial support by MCyT (Spain) under Project No. FIS2007-64698 and Xunta de Galicia (Spain) under Projects No. PGIDIT05PXIC20607PN and No. INCITE07PXI206131ES. We also thank Daniel Cuiñas Vásquez for helpful conversations.

[1] R. J. Briggs, *Electron Stream Interactions with Plasmas* (MIT, Cambridge, MA, 1964).
[2] R. J. Deissler, J. Stat. Phys. **40**, 371 (1985); **54**, 1459 (1989).
[3] M. Kærn and M. Menzinger, Phys. Rev. E **60**, R3471 (1999).
[4] M. Kærn, M. Menzinger, and A. Hunding, J. Theor. Biol. **207**, 473 (2000).
[5] P. V. Kuptsov, S. P. Kuznetsov, C. Knudsen, and E. Mosekilde, *Recent Research Developments in Chemical Physics* (Transworld Research Network, Trivandrum, India, 2003), Vol. 4.
[6] M. Kærn, D. G. Míguez, A. P. Muñuzuri, and M. Menzinger, Biophys. Chem. **110**, 231 (2004).
[7] S. P. Kuznetsov, E. Mosekilde, G. Dewel, and P. Borckmanns, J. Chem. Phys. **106**, 7609 (1997); P. Andresén, M. Bache, E. Mosekilde, G. Dewel, and P. Borckmanns, Phys. Rev. E **60**, 297 (1999).
[8] J. R. Bamforth, S. Kalliadasis, J. H. Merkin, and S. K. Scott, Phys. Chem. Chem. Phys. **2**, 4013 (2000); J. R. Bamforth, J. H. Merkin, S. K. Scott, R. Toth, and V. Gaspar, *ibid.* **3**, 1435 (2001).
[9] M. Kærn, M. Menzinger, R. Satnoianu, and A. Hunding, Faraday Discuss. **120**, 295 (2002).
[10] Y. Bessho and R. Kageyama, Curr. Opin. Genet. Dev. **13**, 379 (2003).
[11] R. A. Satnoianu and M. Menzinger, Phys. Rev. E **62**, 113 (2000); R. Satnoianu, P. K. Maini, and M. Menzinger, Physica D **160**, 79 (2001).
[12] D. D. Miguez, R. A. Satnoianu, and A. P. Muñuzuri, Phys. Rev. E **73**, 025201(R) (2006).
[13] D. G. Miguez, G. G. Izus, and A. P. Muñuzuri, Phys. Rev. E **73**, 016207 (2006).
[14] P. N. McGraw and M. Menzinger, Phys. Rev. E **72**, 026210 (2005).
[15] D. G. Miguez, P. McGraw, A. P. Muñuzuri, and M. Menzinger, Phys. Rev. E **80**, 026208 (2009), the preceding paper.
[16] P. N. McGraw and M. Menzinger, Phys. Rev. E **72**, 027202 (2005).
[17] J. R. Bamforth, R. Tóth, V. Gáspár, and S. K. Scott, Phys. Chem. Chem. Phys. **4**, 1299 (2002).
[18] I. Lengyel, G. Rabai, and I. R. Epstein, J. Am. Chem. Soc. **112**, 9104 (1990).
[19] N. D. Mermin, Rev. Mod. Phys. **51**, 591 (1979); A. Vilenkin, Phys. Rep. **121**, 263 (1985).
[20] P. Andresén, E. Mosekilde, G. Dewel, and P. Borckmans, Phys. Rev. E **62**, 2992 (2000).
[21] M. Kærn and M. Menzinger, Phys. Rev. E **62**, 2994 (2000).
[22] P. N. McGraw and M. Menzinger, Phys. Rev. E **68**, 066122 (2003).
[23] M. Kaern and M. Menzinger, Phys. Rev. E **61**, 3334 (2000).